A&A 531, A119 (2011)
DOI: 10.1051/0004-6361/201015948

Astronomy & Astrophysics

The dark halo of the Hydra I galaxy cluster: core, cusp, cosmological?⋆

Dynamics of NGC 3311 and its globular cluster system

T. Richtler[1], R. Salinas[1,2], I. Misgeld[3], M. Hilker[4], G. K. T. Hau[2], A. J. Romanowsky[5], Y. Schuberth[6], and M. Spolaor[7]

[1] Departamento de Astronomía, Universidad de Concepción, Concepción, Chile
e-mail: [tom; rsalinas]@astro-udec.cl
[2] European Southern Observatory, Alonso de Córdova 3107 Santiago, Chile
[3] Sternwarte der Universität München, Scheinerstr.1, 81679 München, Germany
e-mail: imisgeld@mpe.mpg.de
[4] European Southern Observatory, Karl-Schwarzschild-Str.2, Garching, Germany
e-mail: mhilker@eso.org
[5] UCO/Lick Observatory, University of California, Santa Cruz, CA 95064, USA
e-mail: romanow@ucolick.org
[6] Argelander Institut für Astronomie, Auf dem Hügel 71, 53121 Bonn, Germany
e-mail: yschuber@astro.uni-bonn.de
[7] Australian Astronomical Observatory, PO Box 296, Epping, NSW 1710, Australia
e-mail: max.spolaor@gmail.com

Received 18 October 2010 / Accepted 9 March 2011

ABSTRACT

Context. Some galaxy clusters exhibit shallow or even cored dark matter density profiles in their central regions rather than the predicted steep or cuspy profiles, conflicting with the standard understanding of dark matter. NGC 3311 is the central cD galaxy of the Hydra I cluster (Abell 1060).

Aims. We use globular clusters around NGC 3311, combined with kinematical data of the galaxy itself, to investigate the dark matter distribution in the central region of Hydra I.

Methods. Radial velocities of 118 bright globular clusters, based on VLT/VIMOS mask spectroscopy, are used to calculate velocity dispersions which are well defined out to 100 kpc. NGC 3311 is the most distant galaxy for which this kind of study has been performed. We also determine the velocity dispersions of the stellar component from long-slit spectroscopy of NGC 3311 acquired with VLT/FORS1 out to 20 kpc. We present a new photometric model for NGC 3311, based on deep VLT/FORS1 images in the V-band. We search for a dark halo that, in the context of a spherical Jeans model, can reproduce the kinematical data. We also compare the radial velocity distributions of globular clusters and planetary nebulae.

Results. The projected stellar velocity dispersion rises from a central low value of about 185 km s^{-1} to 350 km s^{-1} at a radius of 20 kpc. The globular cluster dispersion rises as well from 500 km s^{-1} at 10 kpc to about 800 km s^{-1} at 100 kpc, comparable to the velocity dispersion of the cluster galaxies. A dark matter halo with a core (Burkert halo) closely reproduces the velocity dispersions of stars and globular clusters simultaneously under isotropy. The central stellar velocity dispersions predicted by cosmological NFW halos do not agree well with those observed, while the globular clusters allow a wide range of halo parameters. A suspected radial anisotropy of the stellar population found in merger simulations aggravates the disagreement with observations. A slight tangential anisotropy would enable the data to be more accurately reproduced. However, we find discrepancies with previous kinematical data that we cannot resolve, which may indicate a more complicated velocity pattern.

Conclusions. Although one cannot conclusively demonstrate that the dark matter halo of NGC 3311 has a core rather than a cusp, a core seems to be most consistent with the present data. A more complete coverage of the velocity field and a more thorough analysis of the anisotropy is required to reach firm conclusions.

Key words. galaxies: individual: NGC 3311 – galaxies: kinematics and dynamics – galaxies: star clusters: general – galaxies: clusters: individual: Hydra

1. Introduction

Cosmological simulations of dark matter halos of galaxies predict that the density profiles in the very inner regions are *cuspy*, i.e. the density reaches very high values for small radii, and the logarithmic density slope takes the value −1 (the NFW profile; e.g. Navarro et al. 2004) or even smaller, e.g. Bullock et al. (2001), Diemand et al. (2005). This prediction, however, has been found to disagree with observations of low-surface brightness galaxies (see de Blok 2010 for a review). The density profiles have instead been found to be more accurately described by a *core*, i.e. for which the central logarithmic density slope is zero. Brighter galaxies are baryon dominated in their centers, thus the inner dark matter density slopes of bright spirals and ellipticals

⋆ Based on observations taken at the European Southern Observatory, Cerro Paranal, Chile, under the programs 082.B-0680, 076.B-0154, 065.N-0166, 065.N-0459.

are more difficult to determine. However, there is some evidence of cuspy halos in early-type galaxies (Tortora et al. 2010).

Since dark matter halos are self-similar, one also expects to find cuspy dark halos on the larger scales of galaxy groups and galaxy clusters. The most suitable test objects are central cD galaxies of central low surface brightness. For example, Kelson et al. (2002) investigated NGC 6166, the central galaxy of Abell 2199, using long-slit spectroscopy reaching out to 60 kpc. They found that the observations were more accurately represented by a halo with a large core rather than being cuspy. Sand et al. (2004, 2008), using strong and weak lensing models together with the kinematics of the central galaxies, found for the clusters Abell 383 and MS 2137-23 shallow dark matter profiles that are incompatible with the steep NFW slope. The same result emerged from a study of the lens properties of Abell 611 (Newman et al. 2009) (see also Newman et al. (2011) for an improved analysis of Abell 383).

These are important observations, illustrating some fundamental inadequacy of the our present understanding of dark matter which it is therefore of great interest to investigate using a variety of dynamical tracers.

In this context, NGC 3311, the central galaxy of Abell 1060, is one of the most attractive targets. It is the nearest cD galaxy, has a low surface brightness, and has an extremely rich globular cluster system, (e.g. Wehner et al. 2008), providing a wealth of very bright globular clusters that can be used as dynamical tracers. NGC 3311 is probably the most distant galaxy for which this kind of study can currently be performed. We measured the radial velocities of about 120 globular clusters, and simultaneously used long-slit spectra of NGC 3311 itself to investigate the kinematics of the stellar body. Our objective is to describe the stellar kinematics and the GC kinematics consistently with the same dark halo model.

We adopt a distance modulus of 33.4 (a value close to the mean given by NED), corresponding to 47.9 Mpc and a scale of 232 pc/arcsec.

2. Observations and data

Observations and reductions of all data used here are presented extensively in parallel or previous contributions, and here we provide only a brief summary. The globular cluster data were taken with VLT/VIMOS on Cerro Paranal in service mode. We merged two VIMOS programmes, using multi-slit masks with the medium resolution grism. Details of the observations, data reduction, and derivation of radial velocities are described by Misgeld et al. (2011). The VLT/FORS1 images in the V-band that provide the photometric model of NGC 3311, are discussed in Misgeld et al. (2008). The long-slit spectra were obtained using VLT/FORS1 at Cerro Paranal, using the grism 600B. Observations and data reduction are described in detail by Spolaor et al. (2011). A preliminary account of the long-slit data was given by Hau et al. (2004).

3. Ingredients for a Jeans-analysis: photometric model and kinematics

3.1. Photometric model for NGC 3311

We derive the light profile of NGC 3311 by applying IRAF/ELLIPSE in an iterative manner, subtracting during each iteration the contributing light of the neighbouring galaxy NGC 3309 until its residual light was not longer noticeable.

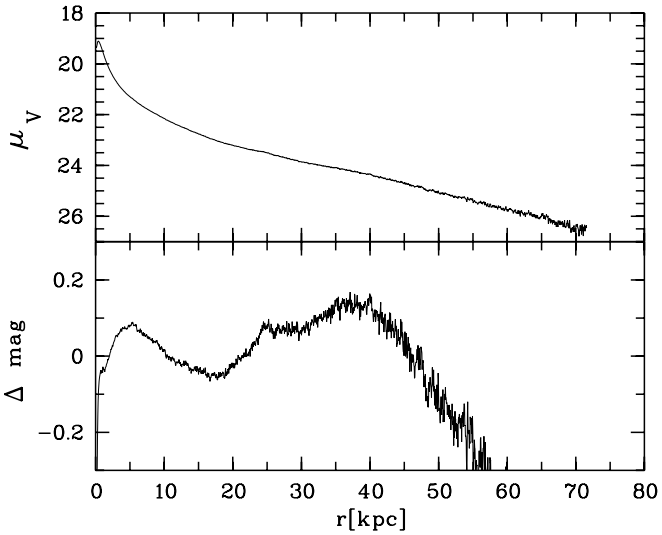

Fig. 1. *Upper panel*: surface-brightness profile in the V-band. *Lower panel*: residuals in mag between our measurements (*upper panel*) and the photometric model in the sense: model−observations.

Since we wish to consider an analytical expression for the projected light that also permits us to perform an analytical deprojection and to calculate an analytical cumulative luminosity, we select a double beta-model for the surface brightness (see also Schuberth et al. 2010) for which we obtain

$$\mu_V(R) = -2.5 \log\left(a_1\left(1+\left(\frac{R}{r_1}\right)^2\right)^{\alpha_1} + a_2\left(1+\left(\frac{R}{r_2}\right)^2\right)^{\alpha_2}\right), \qquad (1)$$

where $a_1 = 2.602 \times 10^{-8}$, $a_2 = 1.768 \times 10^{-9}$, $r_1 = 5''$, $r_2 = 50''$, and $\alpha_1 = \alpha_2 = -1.0$. To transform this surface brightness into $L_\odot/\mathrm{pc}^2$, one has to apply a factor 3.7×10^{10} to the argument of the logarithm. An additional factor 1.27 corrects for the extinction in the V-band (Schlegel et al. 1998).

In its upper panel, Fig. 1 shows the measured surface brightness, and in its lower panel the difference of our photometric model from the measurements in the sense measurements minus the model.

Out to 50 kpc, the representation is excellent, the largest residuals being 0.1 mag. The model then becomes gradually brighter. However, this happens at such faint magnitudes that neither the deprojection nor the cumulative luminosity are significantly affected. Furthermore, the accuracy of the photometry may be questioned. While the low central surface brightness of NGC 3311 and its extended light profile (besides its central position) are characteristics of a cD-galaxy, we cannot identify an inflection point (Kormendy & Djorgovski 1989) that would mark a transition between a normal elliptical galaxy and a halo with a shallower light profile. For example, the difference with NGC 1399 in the Fornax cluster is the larger core of the NGC 3311 light profile. At large radii, both profiles decline approximately as R^{-2} (Dirsch et al. 2003).

3.2. Globular clusters: dispersion and number density profile

We measured radial velocities for 118 bright globular clusters (GCs) in the absolute magnitude range $-13.4 < M_V < -10$. We use this label for simplicity, although the vast majority of these objects can also be named "ultracompact dwarfs" (e.g. Mieske et al. 2009). Figure 2 (left panel) displays the velocities versus

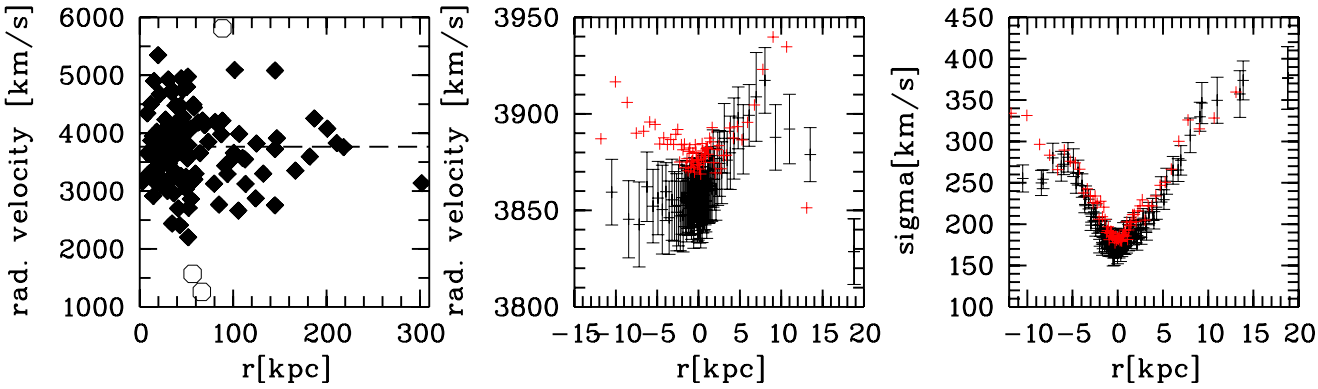

Fig. 2. *Left*: radial velocities of globular clusters (see Sect. 3.2). The horizontal dashed line is the mean heliocentric velocity of globular clusters inside 50 kpc which is 3765 km s^{-1}. *Middle*: radial velocity of NGC 3311 along the major axis (black crosses with error bars) and the minor axis (red crosses) (see Sect. 3.4). *Right panel*: velocity dispersion of NGC 3311 along minor and major axis.

galactocentric distance. While for distances less than 60−70 kpc the velocity dispersion seems to be statistically well defined, this is not the case for larger distances. It is clear that the removal of the two objects near 5000 km s^{-1} with distances 100 kpc and 120 kpc would lower the dispersion considerably. However, a sudden drop in the dispersion beyond 100 kpc does not seem physical. Moreover, the velocity dispersion of the cluster galaxies is about 800 km s^{-1} at 100 kpc (Łokas et al. 2006), which suggests that the outer GC dispersion is of similar order. We consider the three open circles as obvious outliers and do not include them in the dispersion calculation. We regard, however, these these objects as interesting (see the remarks in Sect. 3.6). Here we only consider the full GC sample. Subsamples are discussed in Misgeld et al. (2011).

The upper panel of Fig. 4 shows the corresponding dispersion values and their uncertainties for seven overlapping bins. Their widths of 1.5−2 arcmin ensure that each bin contains about 30 objects (the two outermost bins have widths of 6 and 16 arcmin, respectively), enabling a solid statistical definition of the velocity dispersion (with the caveat given above for large radii). The velocity dispersions were determined using the estimator of Pryor & Meylan (1993). For a Jeans-analysis, we need the number density profile of the GCs that we adopt from Wehner et al. (2008), but their study reaches only to 3′ and thus must be extrapolated to larger radii. For a convenient deprojection, we fit their density profile to a Hubble-Reynolds law (see e.g. Schuberth et al. 2010; Eq. (11)) and obtain for the surface density

$$N(r) = 3.86(1 + (r/8.2\ \mathrm{kpc})^{-2})^{-0.7}, \quad (2)$$

where $N(r)$ is the number per kpc^2.

3.3. The role of NGC 3309 and remarks on the validity of equilibrium

One might suspect that there is a certain level of contamination of the cluster system of NGC 3311 by clusters from the nearby giant elliptical NGC 3309, which has a projected distance of only 100″ from NGC 3311. Harris et al. (1983) and McLaughlin et al. (1995) estimated this contamination globally to be small considering the huge cluster system of NGC 3311. Wehner et al. (2008) quote 16500 ± 2000 as the total number of NGC 3311 clusters in comparison to only 374 ± 210 for NGC 3309, which means an abnormally low specific frequency of about 0.9 for NGC 3309. This suggests that NGC 3309 might have lost part of its original cluster system to NGC 3311. The pair NGC 3311/NGC 3309 bears some resemblance to the central pair NGC 1399/NGC 1404 in the Fornax cluster with NGC 1404 being also being underabundant in globular clusters (Richtler et al. 1992) and clusters actually belonging to NGC 1404 indeed contaminating the cluster system of NGC 1399 (Schuberth et al. 2010). However, our sample of NGC 3311 clusters consists exclusively of very bright objects that are genuinely sparse in normal ellipticals, so we expect the contamination by NGC 3309 to be even lower than the 2% quoted by Wehner et al. (2008).

An additional difference of NGC 1399/NGC 1404 is visible in the X-ray isophotes. At radii larger than 8 kpc, the X-ray isophotes of NGC 1404 are distorted (Paolillo et al. 2002), which indicates the spatial proximity of NGC 1404 to NGC 1399, while no distortion is visible in the isophotes of NGC 3309 observed with Chandra (Yamasaki et al. 2002) and *XMM-Newton* (Hayakawa et al. 2006) These observations support the assumption that NGC 3311 is at the center of the cluster potential and NGC 3309 is spatially at a larger distance from NGC 3311 than the projected distance. Yamasaki et al. also point out the good isothermality (the *XMM-Newton* temperature slightly decreases) and apparent equilibrium of the X-ray gas in NGC 3311. Signs of an ongoing merger are at least indistinguishable. This is in line with the relative distance between NGC 3309 and NGC 3311 given by Mieske et al. (2005) using surface brightness fluctuations. NGC 3309 appears to be somewhat in the foreground.

The assumption of spherical equilibrium for both the NGC 3311 cluster system and Abell 1060 as a whole is probably invalid to a certain degree. The notion of Fitchett & Merritt (1988) that the galaxy velocity distribution in Abell 1060 is flatter than a Gaussian, still holds with the extended sample of Christlein & Zabludoff (2003). We performed a Shapiro-Wilk W-test for normality and found for 212 galaxies (<6000 km s^{-1}) within a radius of 600 kpc a p-value of 0.003, which corresponds to a non-Gaussian distribution (note that this does not mean non-isotropy: in the galaxy cluster sample of Łokas et al. 2006; Abell 1060 is the most isotropic cluster). Our globular cluster sample, however, gives a p-value of 0.68, which is not inconsistent with a normal distribution.

3.4. Stellar kinematics

We analysed long-slit spectra acquired for both the major axis (PA = 28.9°) and minor axis (PA = 118.9°). The NW-part of the minor axis is influenced by NGC 3309 at radii larger than 10 kpc. The spectra are spatially rebinned to achieve a

constant signal-to-noise-ratio of 40 (major axis) and 30 (minor axis). Both the mean velocity and velocity dispersion were measured employing the penalized pixel fitting (pPXF) method of Cappellari & Emsellem (2004). In the pPXF analysis, stellar templates from the MILES spectral library (Sánchez-Blázquez et al. 2006) are convolved with a Gaussian model (plus higher-order components) of the line-of-sight velocity distribution until the χ^2-deviations become minimal.

Figure 2 (middle and right panel) shows the results. Radial distances are given in kpc with the negative values referring to the SW-part of the major axis and the NW-part of the minor axis. The radial velocity curve (middle) has a slightly asymmetric shape along both axes, perhaps representing a small-scale complex velocity field. The rise in the velocity dispersion (right panel) from a quite low central value of about 180 km s^{-1} to 350 km s^{-1} at 20 kpc (already shown in Hau et al. 2004) resembles the results for NGC 6166 in Abell 2199 (Carter et al. 1999, Kelson et al. 2002) where the dispersion rises to about 600 km s^{-1} at 60 kpc.

The velocity dispersion along the major axis shows some asymmetry as well in the sense that in the SW part it rises slightly faster than in the NE part, also seen in the minor axis. Loubser et al. (2008) also show velocity dispersions for NGC 3311 with a radial limit of 15″(3.5 kpc). Our measurements agree with their values in the common inner region. Ventimiglia et al. (2010) presented the stellar kinematics of NGC 3311 out to 30 kpc. Their interesting interpretation of NGC 3311 is that of a small galaxy embedded in a cluster-bound stellar halo, the transition occurring between 4 and 12 kpc. We plot their outer six bins in the two lower panels of Fig. 4. Their two inner values (from Gemini/GMOS) are compatible with our measurements, while their intermediate values (from VLT/FORS2) are considerably higher. Their outermost value is again compatible with our model prediction (see Sect. 4). Our major-axis slit crosses their FORS2 slit in the NE-quadrant at a radius of about 50″(11.6 kpc). Large azimuthal differences over scales of 10″−20″ would be very surprising. Furthermore, our comparison of the major and minor axis measurements indicate that they are consistent with sphericity, although this will remain unclear until a full map of kinematical data becomes available.

3.5. X-ray gas mass

On the galaxy cluster scale, the dominant baryonic component is the hot X-ray plasma. From various X-ray studies of Abell 1060, we adopt the *XMM-Newton* work of Hayakawa et al. (2006) and neglect that their adopted distance is slightly smaller (45.6 Mpc). One finds the gas mass by numerical integration over a beta-profile for the gas density

$$M_{\rm gas} = 4\pi n_0 \mu m_{\rm p} \int_0^r (1 + (z/r_{\rm c})^2)^{-\frac{3}{2}\beta} z^2 {\rm d}z \qquad (3)$$

where $n_0 = 11.7$ cm^{-3} is the central electron density, $\mu = 0.6$ the mean molecular weight, $m_{\rm p}$ the proton mass, $r_{\rm c} = 102$ kpc the scale radius, and $\beta = 0.69$.

In the isothermal case with $kT = 3.3$ KeV, the dynamical mass is then given by e.g. Grego et al. (2001)

$$M_{\rm dyn}(r) = 2.5 \times 10^8 \frac{r^3}{r_{\rm c}^2 + r^2} [M_\odot/{\rm pc}^3]. \qquad (4)$$

We note, that this mass profile is not a good description at small radii: within 25 kpc, the stellar mass alone is higher than the dynamical mass. The interpretation of Hayakawa et al. that the central density profile is cuspy, must therefore be seen with caution. We find good agreement with their gas mass profile. However, the gas mass has only a minor influence on the dynamics, but we include it as the main baryonic component on larger scales. The dynamical mass is used in Sect. 4.3.

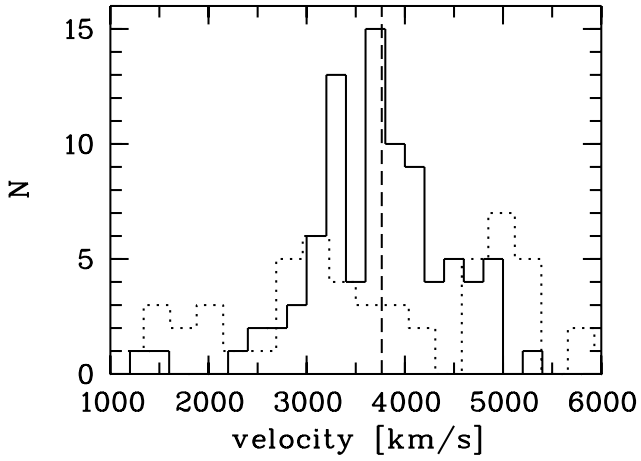

Fig. 3. A comparison of the velocity distributions of globular clusters (GCs; solid histogram) and planetary nebulae (PNe; dashed histogram) from Ventimiglia et al. (2011). The vertical dashed line at 3765 km s^{-1} indicates the mean of all GC velocities. The GCs have projected galactocentric distances that are smaller than 65 kpc in order to match the radial range of PNe. There are striking differences whose origin is not yet understood.

3.6. Comparison of globular cluster velocities with planetary nebulae

During the revision process of this paper, Ventimiglia et al. (2011) published radial velocities of a sample of 56 planetary nebulae (PNe) around NGC 3311. It is therefore appropriate to make a brief comparison between the results for PNe and GCs.

Figure 3 compares the velocity histograms of PNe and GCs inside a radius of 65 kpc which is defined by the radial extent of the PNe sample. The first remark is that the PNe sample is affected even more from small number statistics than the GC sample. Any conclusion has to be confirmed with a larger sample. It is, however, striking that the velocity distribution lacks the peak around the velocity of NGC 3311 that the GC sample shows prominently. Ventimiglia et al. (2011) suggest (along with the speculation that NGC 3311 is intrinsically devoid of PNe) that ram pressure stripping of the PN-shells in the dense parts of the hot X-ray plasma might be responsible for shortening the lifetimes of PNe. In this case, the PNe are sampled outside a cavity around NGC 3311. The questions which remain are why this effect should remove the velocity peak and why this is visible neither in NGC 1399 (McNeil et al. 2010) nor in M 87 (Doherty et al. 2009) where the gas densities are of comparable order. One could add the speculation that the PNe originate in different stellar parent populations, which are perhaps partly of intermediate-age and related to the earlier infall of (dwarf?)-galaxies.

The peak at 3300 km s^{-1} in the GC distribution is not trustworthy within the present sample. Only a few more objects with velocities of about 3500 km s^{-1} would suffice to erase it. However, there is a similarity between the motions of PNe and GCs at larger radii than 100 kpc. As visible in Fig. 2, there

seems to be a bias towards velocities below the systemic velocity. Whether this the effect of the small sample size or not, must be investigated using a larger sample.

It is interesting to consider the occurrence of PNe with velocities smaller than 1500 km s^{-1} in which range two GCs are also found (1293 km s^{-1} and 1570 km s^{-1}, Misgeld et al. 2011). These are deviations of partly more than 3σ for a Gaussian distribution centered on NGC 3311, corresponding to a probability of 0.1% or less. For the GCs it is already improbable to have objects at this velocity, for the PNe due their smaller sample and three objects even more so. The much larger samples of galaxies (Christlein & Zabludoff 2003) and dwarf galaxies (Misgeld et al. 2008) do not contain velocities below 2000 km s^{-1}.

The question is therefore whether these low velocities are recession rather than Doppler-velocities. While the existence of stellar populations between galaxy clusters would be intriguing, one will have to await future surveys to confirm this idea. However, very high peculiar velocities are in principle possible. We return to this issue in Sect. 4.4.

4. Dynamical models

We present dynamical models that are solutions of the non-rotating spherical Jeans-equation (see Mamon & Łokas 2005 for a collection of the relevant formulae). They can be considered as good approximations to spherical stellar systems, assuming equilibrium. We assume that NGC 3311 is at rest at the center of the cluster potential. Given the data limitations, we regard our results as a first approximation to the mass distribution that will be refined later both observationally and theoretically.

With the stellar mass component, the gaseous component, and an assumed dark halo, for which we assume various representations, we model the projected velocity dispersions versus projected radius, using the formulae quoted in Mamon & Łokas (2005). We require a dark halo model, which can simultaneously account for the dispersion of the globular clusters and stars.

The upper panel in Fig. 4 shows the dispersion of GCs described in section 3.2. Various models are indicated. All assume $M/L_V = 6$ for the stellar population, which is needed to reproduce the inner stellar velocity dispersion, and which is also close to the expected value for an old metal-rich population such as NGC 3311 (Spolaor et al. 2011). The middle panel shows the velocity dispersion of the stellar population where the same models are indicated. These models assume isotropy for the stellar distribution of orbits. To demonstrate the need for dark matter, the lower solid line is the expected dispersion without a dark halo. The lower panel shows for selected halos the effect of radial and tangential anisotropies. The kinematical data of Ventimiglia et al. (2010) are plotted in the lower two panels.

We now discuss the models individually.

4.1. NFW halos

The dark halo of Abell 1060 was investigated by Łokas et al. (2006) by a Jeans-analysis, using published galaxy velocities. They use NFW halos (e.g. Navarro et al. 2004) that are analytically represented by

$$\rho(r) = \frac{\rho_s}{\frac{r}{r_s}(1+\frac{r}{r_s})^2} \quad (5)$$

where ρ_s and r_s are the characteristic density and radius, respectively. They have the cumulative mass

$$M_{dark} = 4\pi\rho_s r_s^3 \left(\ln((r_s+r)/r_s) - r/(r_s+r)\right) \quad (6)$$

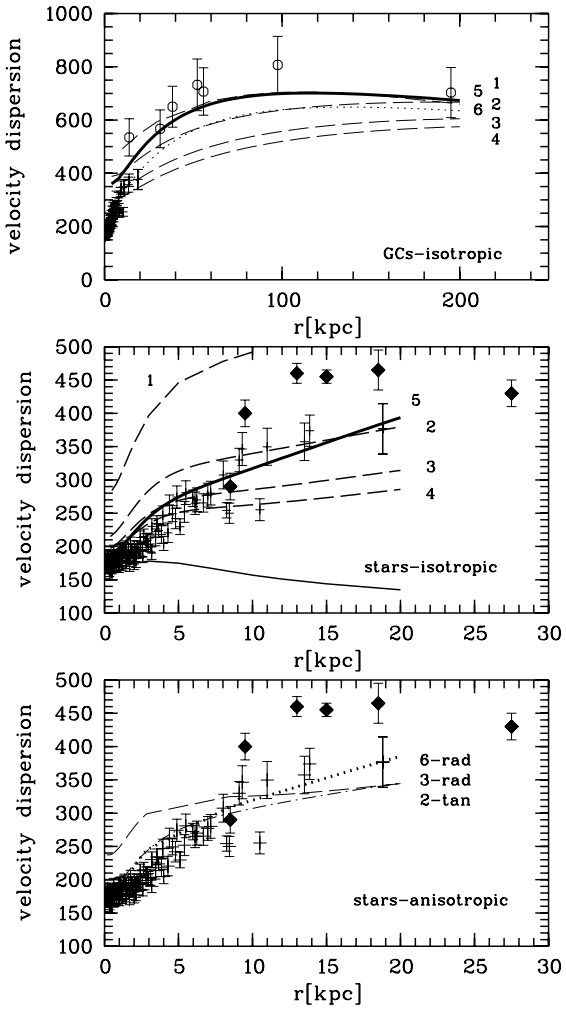

Fig. 4. *Upper panel*: the extended regime of the globular clusters and their velocity dispersions. Open circles denote globular clusters, crosses (which merge together) denote stars. The kinematical data of Ventimiglia et al. (2010) are plotted in the lower two panels see Sect. 3.4 for more details. Six isotropic models (stellar mass+gas mass+dark halo), based on different halo shapes, are indicated. The halo properties are listed in Table 1. Thick solid line (halo 5): a cored halo (Eq. (10)). Dashed lines: NFW halos (Eq. (6)). Numbering is the sequence of vertical order. Halo 1 is the NFW halo quoted by Łokas et al. (2006) from the analysis of galaxy velocities in Abell 1060 (Eq. (6)) (almost coinciding with halo 5). Dotted line (almost coinciding with halo 2): halo 6, which is a cored Burkert halo designed to represent the stars moving with a radial anisotropy. *Middle panel*: the regime of stellar kinematics with isotropic models using the same numbering. The kinematical data of Ventimiglia et al. (2010) are plotted as black diamonds (also in the lower panel). Halo 1 deviates strongly, but is not cosmological according to Macciò et al. (2008). The lower solid line without any number is a model without dark matter for comparison. *Lower panel*: these three models demonstrate the effect of anisotropy of the stellar orbits. Halo 3: radial anisotropy according to Hansen & Moore (2006). Halo 2: constant tangential anisotropy of –0.5. Halo 6 is a Burkert halo with radial anisotropy. See Sects. 4 and 3.4 for details.

It is customary to define a virial radius r_{vir} (which includes the virial mass M_{vir}) inside which the mean density is by a certain factor higher than the critical density of the Universe. This factor is mostly set to 200. Another parameter is the "concentration" $c = r_{vir}/r_s$. Simulations agree in that there is a relation between

Table 1. Properties of dark matter halos in Fig. 4.

ID	$\rho_s[M_\odot/pc^3]$	r_s[kpc]	$M_{vir}[10^{14}M_\odot]$	c	Type
1	0.0072	140	3.87	10.9	NFW
2	0.0013	290	3.97	5.3	NFW
3	0.00051	440	3.94	3.94	NFW
4	0.0003	570	4.05	2.7	NFW
5	0.02	75	2.0 (1 Mpc)	–	Burkert halo (isotropic)
6	0.012	90	1.9 (1 Mpc)	–	Burkert halo (radial)

Notes. Halos 1–4 are of the NFW type (Eq. (6)), halo 5 is a cored Burkert halo (Eq. (10)). Column 1: ID; Col. 2: characteristic density (central density in case of halo 5); Col. 3: scale radius; Col. 4: virial mass (for the Burkert halos the mass within 1 Mpc); Col. 5: concentration; Col. 6: type.

M_{vir} and c, albeit with some scatter. Macciò et al. (2008) quote for that relation (we adopt their Eq. (10) for relaxed halos and set $h = 1$ for convenience)

$$\log\ c = 0.83 - 0.098(\log(M_{vir}/10^{12})). \quad (7)$$

In Fig. 4, the upper panel refers to the regime of globular clusters, the middle panel to the regime of stars, for isotropic models, the lower panel as well to the stars, but with a radial and a tangential model indicated. The numbers always indicate the same halos. For the halo properties, we refer to Table 1.

Halo 1 in Fig. 4 represents the best-fit NFW halo of Łokas et al. (2006) where $\rho_s = 0.0072\ M_\odot/pc^3$, and $r_s = 140$ kpc M_{vir} is $3.87 \times 10^{14}\ M_\odot$, and $c = 10.9$ (note that these values assume a factor of 200 to define the virial mass, while Łokas et al. (2006) use 101.9 and therefore quote $c = 14$). This halo marginally fits the globular clusters, but definitely not the stars. It has a higher concentration than a cosmological halo in the sense of Eq. (7), from where one would expect $c = 3.4$. However, Łokas et al. (2006) give a large uncertainty range for their c-value, which reflects that the galaxies do not strongly constrain the halo shape.

We therefore assume halos that approximately fulfill the Maccio et al.-relation and do not deviate too strongly from the mass quoted by Łokas et al. (2006). Halo 3 is consistent with this relation while halo 2 and 4 are consistent approximately within 1-σ deviations.

Halos 3 and 4 are neither good fits for the globular cluster properties assuming isotropy (upper panel) nor fit the stars beyond about 8 kpc (middle panel). To enable halo 3 to be a closer representation, one could introduce stellar radial anisotropy.

Modest radial anisotropies are common in elliptical galaxies and are also expected from simulations of mergers (Hansen & Moore 2006; Mamon et al. 2006). A radial anisotropy elevates the velocity dispersions, most strongly in the central regions. The prescription of Hansen & Moore (2006) minimizes the central elevation

$$\beta = -0.1 - 0.2\frac{d\ln\rho(r)}{d\ln r}r, \quad (8)$$

where the logarithmic slope of the baryonic mass profile enters, and β is the anisotropy parameter. Our mass profile gives a somewhat complicated behavior, but a very good approximation is given by $\beta = 0.5r/(r_a + r)$ with $r_a = 3$ kpc, which corresponds to Eq. (60) of Mamon & Łokas (2005) and permits us to employ their analytical solutions.

This radial anisotropy for halo 3 is displayed in the lower panel. With some more fine-tuning, one could probably reach a good representation of the stellar kinematics. The problem with globular clusters of course remains.

Halo 2 is so far the most promising, although not really satisfactory. The effect of a slight, radially constant tangential anisotropy of $\beta = -0.5$ is shown in the lower panel. One needs, however, a higher mass and/or a radial anisotropy for the globular clusters. To increase the velocity dispersion at, say, 100 kpc from 600 km s^{-1} to 750 km s^{-1}, one needs approximately to increase the mass by a factor 1.6 (which may be difficult to justify), but then a stronger tangential isotropy and some fine-tuning would then be needed. We note, however, that tangential anisotropies in elliptical galaxies seem to be rare but we refere to NGC 1407 as an example (Romanowsky et al. 2009).

4.2. A cored halo

A more straightforward representation can be achieved by considering a halo with a core instead of a cusp. One could consider the simple density profile $\rho(r) = \rho_0/(1 + (r/r_c)^2)$, ρ_0 being the central density and r_c a scale radius. However, this profile, although it permits a good representation for small radii, corresponds to very high masses at large radii, which deviate strongly from the X-ray mass profile. We therefore use the "Burkert profile" (Burkert 1995), introduced for the dark matter profiles of spiral dwarf galaxies

$$\rho(r) = \frac{\rho_0}{(1 + r/r_c)(1 + (r/r_c)^2)}, \quad (9)$$

whose cumulative mass is

$$M_{dark} = 4\pi\rho_0 r_c^3\left[\frac{1}{2}ln(1+r/r_c)+\frac{1}{4}ln(1+(r/r_c)^2)-\frac{1}{2}\arctan(r/r_c)\right]. \quad (10)$$

This halo is shown in Fig. 4 as the thick solid line (halo 5), and appears to provide the best representation.

To illustrate how the radial anisotropy of Eq. (8) affects this kind of halo, we plot halo 6 in the lower panel (solid thick line) which fits the stars quite well. However, we had to decrease the stellar M/L to 3 in order not to increase the central velocity dispersion. This low M/L-value is not supported by (Spolaor et al. 2011). A radial bias corresponds to a lower halo mass which in turn causes difficulties when fitting the globular clusters.

4.3. Comparison with the X-ray dynamical mass and the halos of other nearby central galaxies

It is interesting to compare the various halos with the X-ray based mass (Hayakawa et al. 2006; Eq. (4)) on larger scales.

Figure 5 shows total mass profiles (stellar mass of NGC 3311 + gaseous mass+dark mass) for halos from Table 1. The thick solid line is the Burkert-halo, the thin solid line is halo 1, and the dashed line is halo 2. With the exception of halo 1, they are in reasonable agreement at large distances with the X-ray based mass. We recall that halo 1 is not clearly defined, so its deviation might not be significant. We also note that the X-ray mass is an extrapolation with the outermost measurement at about 170 kpc. It is amazing that the extrapolation of a small volume of 20 kpc radius still results in sensible masses on the scale of several hundreds of kpc. This uncovers a problem: halo 2 represents a "cosmological" cluster-wide halo, but there is no room anymore for a galaxy-wide halo.

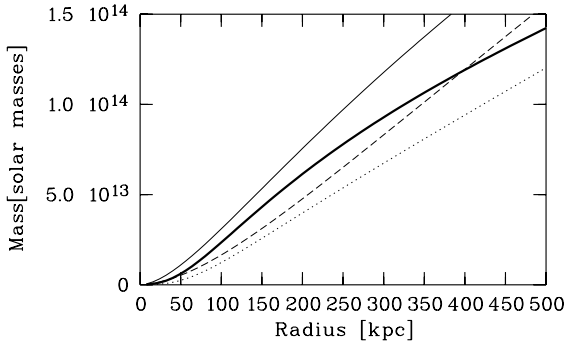

Fig. 5. Mass profiles for some halos from Table 1 compared with the X-ray based mass from Eq. (4) (dotted line). Solid thick line: Burkert halo (halo 5), thin solid line: halo 1, dashed line: halo 2

.

Thus the central dark matter in NGC 3311 "knows" about its location within a galaxy cluster. While this is plausible according to pure dark matter simulations, one should conclude that baryons were not strongly involved in shaping the inner dark matter profile.

A transition between a galaxy halo and a cluster halo has been claimed to be detected in the X-ray profile of NGC 1399, the central galaxy of the Fornax cluster (Ikebe et al. 1996). However, this feature could not be found for the kinematics of the GC system (Schuberth et al. 2010). The best-fit dark halos (see Table 6 of Schuberth et al.) are those that use only the metal-rich GCs. These halos have small core radii and are clearly not cosmological. The metal-poor GCs display a more erratic behaviour and represent halos that are marginally cosmological, but provide poorer fits.

On the other hand, the dark halo of M 87, the central galaxy of the Virgo cluster, which is advocated by Côté et al. (2001) (NFW halo, their Eq. (11)), is similar to our halo 4 with ρ_s = 0.0003 $M_\odot/\mathrm{pc}^3$, r_s = 560 kpc, and c = 2.8.

In conclusion, we do not yet have a uniform picture for the halos of nearby central galaxies.

4.4. Extreme velocities

Some GCs and PNe have radial velocities with offsets of about 2700 km s^{-1} from the mean cluster velocity. Are these orbits consistent with the halo masses? We consider the most favorable case, namely that these velocities are space velocities near their perigalactica. We consider halo 2, neglecting stellar and gas masses. Our GC with the lowest velocity (1259 km s^{-1}) has a projected distance of 66 kpc from NGC 3311. We use an orbit program kindly provided by M. Fellhauer (private communication) to calculate the apogalactic distance if the perigalactic distance is 66 kpc and the perigalactic velocity is 2465 km s^{-1}. The result is an apogalactic distance of 1237 kpc and an orbital period of 2.8 Gyr. These orbits are thus possible, but since it is improbable to pick up an object near its pericenter while its velocity vector points towards the observer, one may expect a larger population of these "intracluster" objects with less inclined orbits. These have also been found among GCs in the Fornax (Schuberth et al. 2010, 2008) and Coma (Peng et al. 2011) galaxy clusters. PNe associated with the intra-cluster light in Hydra I were discussed in Ventimiglia et al. (2008). This agrees with studies finding that the contribution of intracluster stellar populations is considerable, e.g. Gonzalez et al. (2007).

5. Conclusions

The core-cusp controversy regarding the inner shape of dark matter halos in galaxies seems to be far from being resolved. For low surface brightness galaxies, cuspy halos predicted by cosmological simulations, do not find support in the observational data (e.g. de Blok 2010, but see Goerdt et al. 2010 for a means of transforming a cuspy dark matter profile into a cored profile). Therefore, it is of fundamental interest to investigate the more massive halos of galaxy clusters. NGC 3311, the central galaxy in the Hydra I cluster (Abell 1060), appears as an interesting test object because of its low surface brightness which implies that dark matter effects are better visible.

We have used the velocity dispersion profile of the stellar population of NGC 3311 and the 118 radial velocities of bright globular clusters to constrain the shape of the dark matter halo. With simplifying assumptions (equilibrium, sphericity, NGC 3311 at rest), we have found that cuspy dark matter halos of the NFW type, which obey the relation between concentration and virial mass found in cosmological simulations and explain the globular cluster velocity dispersion, do not satisfactorily account for the smooth rise in the stellar velocity dispersion at small radii under isotropy. Halos with a core can more accurately reproduce the stellar and globular cluster kinematics observed for NGC 3311.

A radial anisotropy, which is frequently observed in elliptical galaxies, aggravates the problem for any kind of halo in that the projected velocity dispersions are higher and the halo mass becomes too low to account for the motion of globular clusters. Tangential anisotropies (best a fine-tuned behaviour) could perhaps provide a solution, but they have rarely been found observationally nor are supported by dynamical models of galaxies.

With the present analysis, one cannot exclude the existence of a cuspy halo in NGC 3311, but a cored dark matter halo seems to be more likely.

Our assumptions may be questionable. More sophisticated dynamical modelling of a larger data set (many more velocities, a better knowledge of the structural parameters of the globular cluster system, and a precise two-dimensional velocity field of the NGC 3311 galaxy light) may find slightly different halos. However, the finding of a core would be in line with independent findings of shallow dark matter profiles in galaxy clusters (see introduction). Any resolution of the conflict with the standard knowledge of dark matter must work on very different mass-scales from dwarf galaxies (e.g. Gentile et al. 2007) to galaxy clusters. A comparison with other nearby central galaxies does not yet provide a uniform picture.

The ability of NGC 3311 and other central galaxies of low surface brightness to trace the dark cores of galaxy clusters awaits exciting future work.

Acknowledgements. We thank an anonymous referee for a thoughtful report and particularly for emphasizing the role of the concentration-mass relation of cosmological halos. We thank Michael Fellhauer for providing his orbit program. T.R. acknowledges financial support from the Chilean Center for Astrophysics, FONDAP Nr. 15010003, from FONDECYT project Nr. 1100620, and from the BASAL Centro de Astrofisica y Tecnologias Afines (CATA) PFB-06/2007. I.M. acknowledges support through DFG grant BE1091/13-1. A.J.R. was supported by National Science Foundation grants AST-0808099 and AST-0909237.

References

Bullock, J. S., Kolatt, T. S., Sigad, Y., et al. 2001, MNRAS, 321, 559
Burkert, A. 1995, ApJ, 447, L25
Cappellari, M., & Emsellem, E. 2004, PASP, 116, 138
Carter, D., Bridges, T. J., & Hau, G. K. T. 1999, MNRAS, 307, 131
Christlein, D., & Zabludoff, A. I. 2003, ApJ, 591, 764

Côté, P., McLaughlin, D. E., Hanes, D. A., et al. 2001, ApJ, 559, 828
de Blok, W. J. G. 2010, Adv. Astron., 2010
Diemand, J., Zemp, M., Moore, B., Stadel, J., & Carollo, C. M. 2005, MNRAS, 364, 665
Dirsch, B., Richtler, T., Geisler, D., et al. 2003, AJ, 125, 1908
Doherty, M., Arnaboldi, M., Das, P., et al. 2009, A&A, 502, 771
Fitchett, M., & Merritt, D. 1988, ApJ, 335, 18
Gentile, G., Salucci, P., Klein, U., & Granato, G. L. 2007, MNRAS, 375, 199
Goerdt, T., Moore, B., Read, J. I., & Stadel, J. 2010, ApJ, 725, 1707
Gonzalez, A. H., Zaritsky, D., & Zabludoff, A. I. 2007, ApJ, 666, 147
Grego, L., Carlstrom, J. E., Reese, E. D., et al. 2001, ApJ, 552, 2
Hansen, S. H., & Moore, B. 2006, New Astron., 11, 333
Harris, W. E., Smith, M. G., & Myra, E. S. 1983, ApJ, 272, 456
Hau, G. K. T., Hilker, M., Bridges, T., et al. 2004, in Outskirts of Galaxy Clusters: Intense Life in the Suburbs, ed. A. Diaferio, IAU Colloq., 195, 491
Hayakawa, A., Hoshino, A., Ishida, M., et al. 2006, PASJ, 58, 695
Ikebe, Y., Ezawa, H., Fukazawa, Y., et al. 1996, Nature, 379, 427
Kelson, D. D., Zabludoff, A. I., Williams, K. A., et al. 2002, ApJ, 576, 720
Kormendy, J., & Djorgovski, S. 1989, ARA&A, 27, 235
Łokas, E. L., Wojtak, R., Gottlöber, S., Mamon, G. A., & Prada, F. 2006, MNRAS, 367, 1463
Loubser, S. I., Sansom, A. E., Sánchez-Blázquez, P., Soechting, I. K., & Bromage, G. E. 2008, MNRAS, 391, 1009
Macciò, A. V., Dutton, A. A., & van den Bosch, F. C. 2008, MNRAS, 391, 1940
Mamon, G. A., & Łokas, E. L. 2005, MNRAS, 363, 705
Mamon, G. A., Łokas, E., Dekel, A., Stoehr, F., & Cox, T. J. 2006, in EAS Pub. Ser. 20, ed. G. A. Mamon, F. Combes, C. Deffayet, & B. Fort, 139
McLaughlin, D. E., Secker, J., Harris, W. E., & Geisler, D. 1995, AJ, 109, 1033
McNeil, E. K., Arnaboldi, M., Freeman, K. C., et al. 2010, A&A, 518, A44
Mieske, S., Hilker, M., & Infante, L. 2005, A&A, 438, 103
Mieske, S., Hilker, M., Misgeld, I., et al. 2009, A&A, 498, 705
Misgeld, I., Mieske, S., & Hilker, M. 2008, A&A, 486, 697
Misgeld, I., Mieske, S., Hilker, M., et al. 2011, A&A, 531, A4
Navarro, J. F., Hayashi, E., Power, C., et al. 2004, MNRAS, 349, 1039
Newman, A. B., Treu, T., Ellis, R. S., et al. 2009, ApJ, 706, 1078
Newman, A. B., Treu, T., Ellis, R. S., & Sand, D. J. 2011, ApJ, 728, L39
Paolillo, M., Fabbiano, G., Peres, G., & Kim, D. 2002, ApJ, 565, 883
Peng, E. W., Ferguson, H. C., Goudfrooij, P., et al. 2011, ApJ, 730, 23
Pryor, C., & Meylan, G. 1993, in Structure and Dynamics of Globular Clusters, ed. S. G. Djorgovski & G. Meylan, ASP Conf. Ser., 50, 357
Richtler, T., Grebel, E. K., Domgoergen, H., Hilker, M., & Kissler, M. 1992, A&A, 264, 25
Romanowsky, A. J., Strader, J., Spitler, L. R., et al. 2009, AJ, 137, 4956
Sánchez-Blázquez, P., Peletier, R. F., Jiménez-Vicente, J., et al. 2006, MNRAS, 371, 703
Sand, D. J., Treu, T., Smith, G. P., & Ellis, R. S. 2004, ApJ, 604, 88
Sand, D. J., Treu, T., Ellis, R. S., Smith, G. P., & Kneib, J. 2008, ApJ, 674, 711
Schlegel, D. J., Finkbeiner, D. P., & Davis, M. 1998, ApJ, 500, 525
Schuberth, Y., Richtler, T., Bassino, L., & Hilker, M. 2008, A&A, 477, L9
Schuberth, Y., Richtler, T., Hilker, M., et al. 2010, A&A, 513, A52
Spolaor, M., Hau, G., Hilker, M., Salinas, R., & Richtler, T. 2011, MNRAS, submitted
Tortora, C., Napolitano, N. R., Romanowsky, A. J., & Jetzer, P. 2010, ApJ, 721, L1
Ventimiglia, G., Arnaboldi, M., & Gerhard, O. 2008, Astron. Nachr., 329, 1057
Ventimiglia, G., Gerhard, O., Arnaboldi, M., & Coccato, L. 2010, A&A, 520, L9
Ventimiglia, G., Arnaboldi, M., & Gerhard, O. 2011, A&A, 528, A24
Wehner, E. M. H., Harris, W. E., Whitmore, B. C., Rothberg, B., & Woodley, K. A. 2008, ApJ, 681, 1233
Yamasaki, N. Y., Ohashi, T., & Furusho, T. 2002, ApJ, 578, 833